SOC in Landslides

Stefan Hergarten

Scale invariance at the earth's surface has attracted scientists for several decades. Even the first formal description of scale invariance in nature concerned geomorphic data. In his seminal work, Mandelbrot [1967] measured the length of coastlines with rulers of different lengths and found a power-law relation between the measured length and the ruler's length. The scaling exponent of this power-law relation was used to assign a non-integer dimension between one and two to these lines. The fractional dimension finally led to the term fractals.

In the 1980s, when fractals became popular and subject of several monographs [e.g., Mandelbrot, 1982, Feder, 1988], geomorphology again provided one of the most fascinating examples: artificial self-affine landscapes [e.g., Voss, 1985, Feder, 1988]. Figure 1 shows an example with a local fractal dimension [e.g., Mandelbrot, 1985] $D_l = 2.1$, generated by Fourier methods [e.g., Hergarten, 2002].

Although these artificial surfaces may be beautiful and even somewhat similar to the real topography of the earth at first sight, their value turned out to be limited. First, the earth's surface is not perfectly self-similar or self-affine [Evans and McClean, 1995] as it is shaped by a variety of processes and shows strong correlations between elevation and slope [e. g., Kühni and Pfiffner, 2001] which are not reproduced by simple self-affine surfaces. Furthermore, these surfaces lack important geomorphic elements such as river valleys. And finally, the algorithms behind these surfaces seem to be far away from the present understanding of the tectonic and geomorphic processes shaping the real topography.

A few years after the concept of SOC was introduced, the first attempts to recognize SOC in landform evolution were made [Kramer and Marder, 1992, Takayasu and Inaoka, 1992, Rinaldo et al., 1993]. These studies addressed the statistical properties of river networks using models of fluvial erosion. Scale-invariant properties of river networks were found even before the term fractal was coined [Horton, 1945, Strahler, 1952, Hack, 1957]. The models themselves were similar in their spirit. It

Stefan Hergarten
Institut für Angewandte Geowissenschaften, Technische Universität Graz, e-mail: `stefan.hergarten@uni-graz.at`

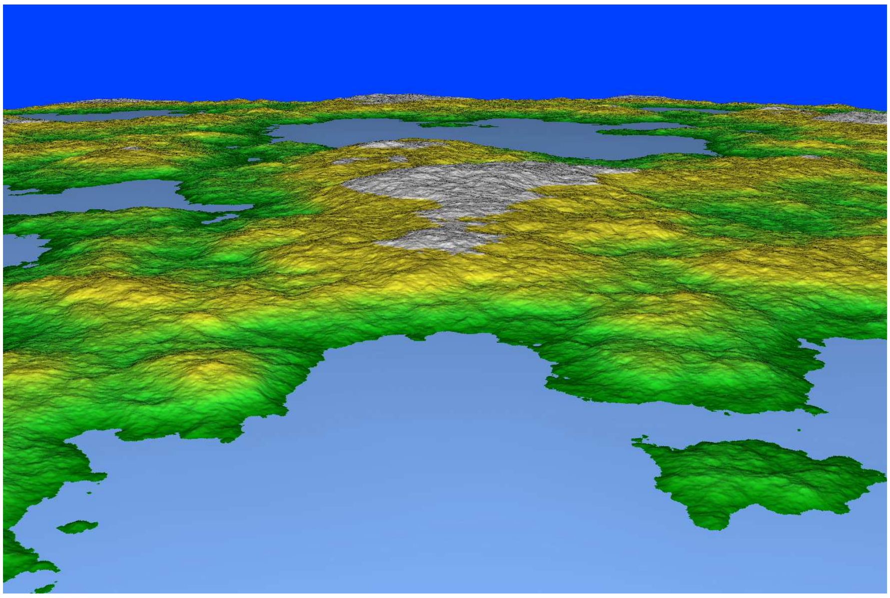

Fig. 1 A computer-generated, self-affine surface with a local fractal dimension $D_l = 2.1$. For a more realistic impression, the landscape was flooded up to a certain level and placed on a section of a sphere in order to improve the aerial view.

was assumed that water takes the direction of the steepest descent on the surface, and that the erosion rate of a river segment depends on the discharge and on the local channel slope. The simplest case addresses the evolution of the topography and the river network under constant tectonic uplift where the surface elevation at one or more pre-defined outlet points at the boundary is kept constant.

It was found that the topography including the river network evolves towards a steady state under these conditions. Figure 2 shows an example of such a tree-like network. The steady-state networks obtained from these models were found to reproduce several statistical properties of real river networks. Furthermore it turned out that the details of the model, i.e., the constitutive law for the erosion rate as a function of discharge and slope, has a minor effect on the statistical properties of the network.

So these models are examples of self-organization towards a steady state with some scale-invariant properties. Takayasu and Inaoka [1992] even entitled this behavior as a new type of SOC. But as pointed out by Sapozhnikov and Foufoula-Georgiou [1996], this kind of self-organization is not SOC. The evolution ends at a steady state without further fluctuations, so that this state is not critical.

However, tectonic forces and thus the uplift rates are not constant at geological timescales, which is one reason that real landscapes do not achieve a steady state. In order to mimic these permanently changing driving forces, Hergarten and Neugebauer [2001] suggested an extended landform evolution model where the lo-

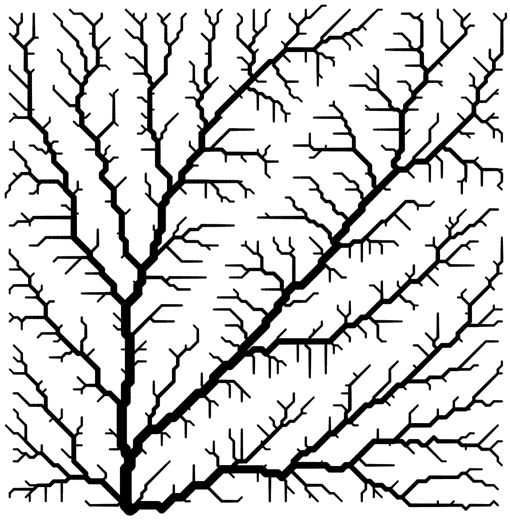

Fig. 2 A simulated river network [Hergarten, 2002].

cation of the outlet is not constant, but varies through time along the boundary of the model domain. As a consequence, the river network permanently changes and never achieves a steady state. These changes are even reflected by a power law if each change in flow direction at any site is considered as a geomorphic event, and if the event sizes are measured in terms of changes in river discharge or, more precisely, catchment size. But unfortunately, it is impossible to verify this event-size distribution in nature. There is indeed evidence for historical changes in the river network even in mountain belts with deep valleys, but only very few events can be clearly recognized, so that a reasonable statistics seems to be out of reach. Even analyzing the changes in braided river systems which evolve very rapidly compared to large-scale river networks may take more than a human lifetime, and the results obtained from downscaled laboratory experiments [Sapozhnikov and Foufoula-Georgiou, 1997] are non-unique with regard to SOC.

So it seems that large-scale landform evolution is in principle unsuitable for recognizing SOC. The rest of this chapter is devoted to landslides which constitute a major natural hazard in almost all mountainous regions and are the presumably the geomorphic process which is most widely studied in the context of SOC.

1 Landslide Statistics

Landslides cover an enormous range of scales and a variety of phenomena. In the vast majority of the literature the term landslides is used as a synonym for all gravity-driven mass movements. The involved masses may be either rock fragments or an unconsolidated regolith layer (mainly soil). Depending on the topographic characteristics and the properties of the material, the motion may be dominated by flow, sliding, avalanching, toppling of falling.

The smallest noticeable landslides are rockfalls with a volume in the order of magnitude of 10^{-3} m^3. However, mass movements involving several million cubic meters occur quite frequently. Figure 3 shows a rockslide with a volume of about 3×10^7 m^3 that took place in the Matter valley in the Swiss Alps in 1991. Only about 50 years ago, a block of more than one quarter cubic kilometer detached above the Vaiont reservoir in the Dolomite Region of the Italian Alps from a wall and slid into the lake at velocities of up to 30 meters per second. As a result, a wave of water overtopped the dam and swept onto the valley below, with the loss of about 2500 lives. The largest rockslide documented in the European Alps, the Flims rockslide, is even more than 30 times larger with respect to volume than the Vaiont reservoir disaster. Estimates of its total volume cover the range from 8 to 15 km^3 [e.g., von Poschinger, 2011].

Fig. 3 Debris deposits of a rockslide in the Matter valley (Swiss Alps).

Extensive landslide statistics have been collected for several decades. More than 40 years ago, Fuyii [1969] found a power-law distribution in 650 events induced by heavy rainfall in Japan. In a more comprehensive study, Hovius et al. [1997] analyzed about 5000 regolith landslides in the western Southern Alps of New Zealand. Malamud et al. [2004] compiled regolith landslide data sets from several regions, each of them consisting of about 1000 to 45,000 events. Some of them were derived from historical inventories, while other consist of events attributed to one triggering event (rapid snowmelt, a rainstorm or an earthquake).

Figure 4 shows the frequency density of eight data sets taken from Hovius et al. [1997] and Malamud et al. [2004] where the area is used as a measure of landslide size. The diagram displays the frequency density, which is simply the product of the probability density and the total number of events. It can be estimated by collecting the objects in (here logarithmic) bins and dividing the number of objects in each bin by the bin width.

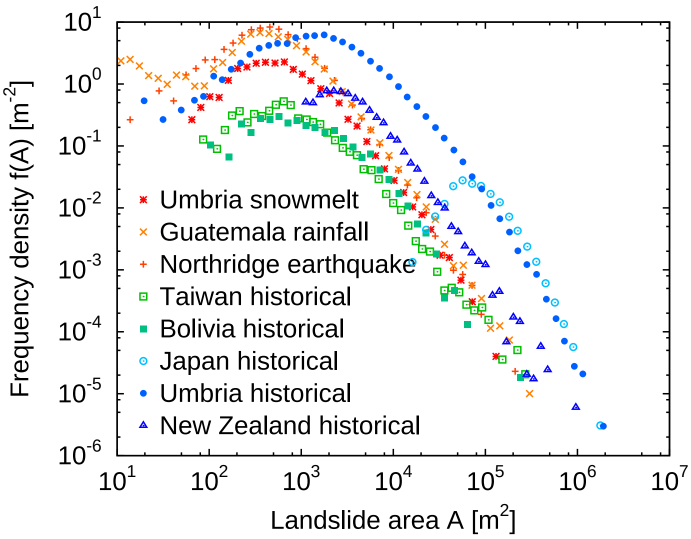

Fig. 4 Frequency density of eight landslide data sets [Hovius et al., 1997, Malamud et al., 2004].

Malamud et al. [2004] found a power-law distribution

$$f(A) \propto A^{-\alpha_A}, \tag{1}$$

with a scaling exponent $\alpha_A \approx 2.4$ at large landslide sizes and a rather small variation between the considered data sets. In particular, there seems to be not systematic difference between the statistics of the landslides triggered by a single earthquake, rainstorm or snowmelt event (red/orange in Fig. 4) and historical inventories involving events arising from various triggers (green/blue).

All datasets displayed in Fig. 4 reveal a striking deviation from a power law at small sizes. The rollover of at small sizes indicates a lack of small landslides in all data sets. Although Malamud et al. suggested a function to describe it quantitatively, its origin is still unclear, but it seems not to be an artefact of incomplete sampling. This rollover strongly limits the range of landslide sizes where a power law can be found since the largest events are in the order of magnitude of 1 km^2 and thus occur at very low frequencies. As a result, none of the distributions shows a clear power law over more than two decades in area, which is only one decade in linear size.

Compared to the distributions of earthquakes (Chapter 9) and wildfires (Chapter 10) this is a rather narrow range.

Available statistics of rock mass movements are much smaller than the inventories of regolith landslides. Malamud et al. [2004] re-analyzed three inventories of rockfalls and rockslides originally published by Dussauge et al. [2002]. Each data set consists of only 89 to 157 events compared to several thousands in the landslide inventories. The frequency densities are displayed in Fig. 5. While landslide size was measured in terms of area, volume is used here.

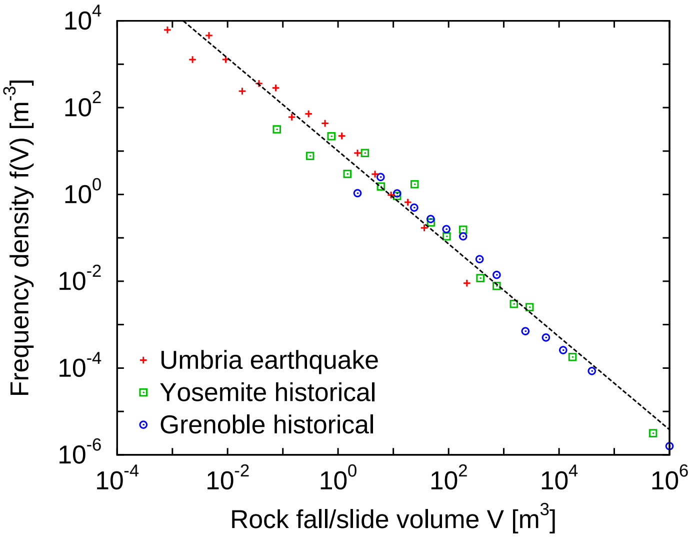

Fig. 5 Frequency density of three rockfall inventories [Dussauge et al., 2002, Malamud et al., 2004]. The dashed line illustrates a power law with a scaling exponent of 1.07.

In contrast to the landslide statistics shown in Fig. 4, no obvious rollover at small sizes is visible here. Consequently, the power-law distribution extends over a larger range of scales, about 5 to 7 decades in volume for each data set. Malamud et al. found that a power law with a scaling exponent $\alpha_V = 1.07$ fits well to the three datasets without any vertical shift of the curves. This result suggests that the power law even extends over 9 orders of magnitude, but fitting one power-law distribution to a merged data set is in principle dangerous as it strongly depends on the number of events in each data set. However, simultaneously fitting three power-law distributions with the same scaling exponent, but different factors in front of the power law confirms the result $\alpha_V = 1.07$.

As reviewed by Brunetti et al. [2009], similar power-law distributions of rockfall and rockslide volumes were found in several other studies. Applying different methods of analysis in different regions on Earth, exponents $\alpha_V = 1.1$ [Guzzetti et al., 2003], $\alpha_V = 1.2$ [Guzzetti et al., 2004], $\alpha_V = 1.19$–1.23 [Noever, 1993], $\alpha_V =$ 1.41–1.52 (the original results of Dussauge et al. [2002] re-analyzed by Malamud et al. [2004], and $\alpha_V = 1.40$–1.72 [Hungr et al., 1999] were obtained. Except for two data sets which address rather small scales, all these values fall into the range $1.07 \leq \alpha_V \leq 1.52$. So the finding that a variation of more than 0.4 in α_V was obtained by applying different methods to the same data sets [Dussauge et al., 2002, Malamud et al., 2004] suggests that the entire variation in α_V may be a spurious effect of limited statistics.

In addition to an apparent independence on the triggering mechanism, no significant difference between rockfalls and rockslides was revealed. Following the majority of the references cited in this paper, the term rockfalls is therefore used for all types of rapid rock mass movements, in particular rockfalls and rockslides, in the rest of this chapter.

When comparing scaling exponents obtained for rockfalls with those obtained for regolith landslides, we must either transform the area-related regolith landslide distributions to volumes or the volume-related rockfall-size distributions to areas. The simplest assumption is isotropic scaling, $V \propto A^{\frac{3}{2}}$, as used, e.g., by Hovius et al. [1997] for regolith landslides. However, non-isotropic scaling was revealed in a comprehensive theoretical study by Klar et al. [2011], as it was also found much earlier in field studies [e.g., Simonett, 1967]. Klar et al. found a weaker increase of volume with area, $V \propto A^{\gamma}$ with $\gamma \in [1.32, 1.38]$, in very good agreement with field observations. Then, comparing the cumulative distributions with respect to area and volume immediately leads to the relation

$$\alpha_A - 1 = \gamma(\alpha_V - 1)\,, \tag{2}$$

and thus for $\gamma \leq 1.4$

$$\alpha_V \geq \frac{\alpha_A - 1}{1.4} + 1 \approx 2.0 \tag{3}$$

for regolith landslides ($\alpha_A \approx 2.4$). This value is clearly larger than the range $1.07 \leq \alpha_V \leq 1.52$ found in the rockfall inventories.

In summary, there is growing evidence for power-law size statistics in both regolith landslides and rockfalls (including rockslides). Neither significant regional variations in the scaling exponent nor a dependence on the triggering mechanism has been found. However, the values of the scaling exponent of rockfall size distributions are significantly smaller than those found for regolith landslides.

2 Mechanical Models

The power-law distributions found for landslide sizes suggest a relationship to SOC. In the following, the most important modeling approaches in this context are discussed.

All these models address the mobilization of rock or regolith masses. With respect to hazard assessment, this is only half of the story because the runout of a mass movement is as important as the initial mobilization. In particular, debris flows consisting of a mixture of rock and water may travel over distances of several kilometers. Rockfalls, rockslides, and rock avalanches may also differ strongly in their runout behavior. Reviews on models predicting the runout of rock mass movements are given by, e.g., Dorren [2003] and Volkwein et al. [2011]. In principle the runout may affect the size distribution of the landslides, too. First, rockfall and rockslide inventories mostly refer to the deposited volume which is in general larger than the detached volume as the compactness of the material decreases during the movement. And second, the volume may also increase due to the entrainment of further rock masses. However, dilatancy should not vary strongly with the event size, and the second effect becomes significant for a small class of mass movements only. Under these aspects it seems to be reasonable that the models attempting to relate landslides to SOC only address the detached volumes or the related areas.

The stability of slopes and cliffs is a mechanical problem involving stresses mainly induced by gravity, but in some cases also by variations in temperature or pore water pressure. In rock, pre-defined fracture patterns may be of particular importance, while existing zones of weakness (e.g., clay layers) may strongly affect the stability of a regolith layer. The topography defines the boundary condition for the 3-dimensional mechanical problem and is thus at least as important as the mechanics inside the domain. Although this is all clear on a qualitative level, and even the differential equations behind it seem to be well-known, the question whether the power-law distribution arises from an evolving fracture pattern (in rock), another type of stress redistribution or the topography changing through type is still open.

In this section, two models addressing the redistribution of stress are discussed. Both are reduced to two dimensions and in principle concern the stability along a pre-defined slip surface as it is often found in regolith landslides. Topography is not directly considered in these models. In their spirit, both models can be seen as extensions of the classical limit equilibrium approach going back to W. Fellenius in the 1920s. The factor of safety FS of a given slip surface is defined as the ratio of maximum shear stress $\tau_{\max}$ where the material remains stable and the actual shear stress τ,

$$FS = \frac{\tau_{\max}}{\tau}, \tag{4}$$

so that the slope remains stable as long as $FS \geq 1$.

The models discussed in the following extend this approach by progressive failure using a local factor of safety. If $FS < 1$ at any location, local failure occurs and leads to an increase of τ and thus to a decrease of FS in the neighborhood. This idea is basically the same as the idea behind the Burridge-Knopoff earthquake model [Burridge and Knopoff, 1967] and its most widespread cellular automaton version, the Olami-Feder-Christensen (OFC) model [Olami et al., 1992]. Altough 20 years old, this model ist still one of the most widely studied models in the field of SOC, and it is discussed in detail in almost all books on SOC [e.g., Bak, 1996, Jensen, 1998, Hergarten, 2002]. Figure 6(a) illustrates a physical realization of the OFC model. A set of blocks on a regular lattice is interconnected by springs and held by static friction at the ground. The force $u_{i,j}$ acting on each block increases through time due to an additional connection with a rigid upper plate moving at a constant velocity. When the force acting on a site reaches the limit of friction, the site becomes unstable and is immediately displaced to a new position characterized by zero total force. As a result, a fraction α of the force $u_{i,j}$ is transferred to each of the four nearest neigbors, leading to the relaxation rule of the OFC model

$$u_{i\pm1,j} := u_{i\pm1,j} + \alpha\, u_{i,j}, \quad u_{i,j\pm1} := u_{i,j\pm1} + \alpha\, u_{i,j}, \quad \text{and} \quad u_{i,j} := 0. \tag{5}$$

Here, the symbol $:=$ means that the value of the variable is replaced with the value at the right-hand side. As a part of the force is transferred to the upper plate (depending on the constants of the springs), α must be smaller than one quarter, making the model nonconservative.

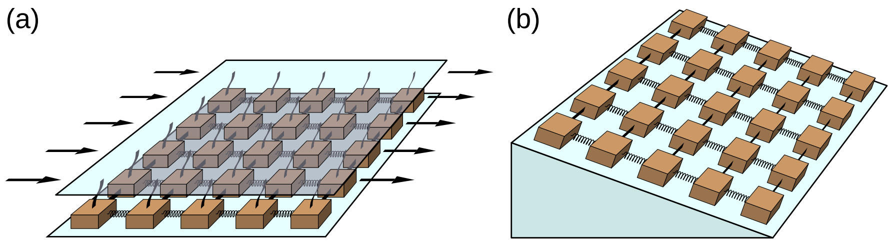

Fig. 6 (a) Geometric representation of the Olami-Feder-Christensen earthquake model. (b) Transfer of the idea to simulate progressive slope failure at a given slip surface.

The long-term driving introduced by a rigid upper plate in the earthquake model mimics the long-term displacement between the walls of a geological fault or a subduction zone. Such a way of driving is obviously absent in case of landslides, so that the driver plate has been removed in the realization shown in Fig. 6(b). Instead, the blocks connected by elastic springs have been placed on an inclined surface, resulting in a constant driving force in downslope direction.

But apart from the different way of long-term driving, the absence of the rigid driver plate also affects the rule of relaxation in case of local instability. In the earthquake model, the relaxed stress is redistributed among the 4 nearest neighbor sites and the driver plate, and the proportion depends on the strength of the springs. Thus, the relaxation within the lattice of blocks is nonconservative. This property is crucial for reproducing the size-distribution of real earthquakes as the scaling exponent of the event-size distribution roughly approaches 1.2 [e.g., Hergarten, 2002] in the conservative limit, which is much too low. Without the driver rigid upper plate, the redistribution of stress becomes conservative, and then the scaling exponent of about 1.2 is clearly too far off from the value $\alpha_A \approx 2.4$ found for regolith landslides.

As the conservative character of the model stems from the principle of conservation of momentum, Hergarten and Neugebauer [2000] looked for a way to obtain larger scaling exponents under conservative stress transfer. They extended the model by a component of time-dependent weakening, which means that the threshold of instability decreases through time between events and is reset after each event.

The model involves two local variables $u_{i,j}$ and $v_{i,j}$ defined on a quadratic lattice. The variable $u_{i,j}$ relaxes conservatively in case of instability like the stresses in the model shown in Fig. 6(b) would do. In return, $v_{i,j}$, describing time-dependent weakening, is locally reset to zero in case of instability without any transfer to the neighbors:

$$u_{i\pm1,j} := u_{i\pm1,j} + \frac{1}{4}u_{i,j}, \quad u_{i,j\pm1} := u_{i,j\pm1} + \frac{1}{4}u_{i,j}, \quad u_{i,j} := 0\ , \qquad \text{and} \quad v_{i,j} := 0\ . \tag{6}$$

Between events, both variables increase at given rates:

$$\frac{d}{dt}u_{i,j} = r_u \quad \text{and} \quad \frac{d}{dt}v_{i,j} = r_v. \tag{7}$$

The rate r_u may describe an increase of stress due to long-term changes in topography, while r_v quantifies the rate of weakening through time. It was assumed that slope stability depends on the product of both variables, i.e., that a site becomes unstable if

$$u_{i,j}v_{i,j} \geq 1. \tag{8}$$

So the model can be directly transferred to the factor of safety approach (Eq. 4) by defining $u_{i,j} = \tau$ and $v_{i,j} = \frac{1}{\tau_{\max}}$ locally. The latter means that, as long as the slope remains stable, the threshold shear stress $\tau_{\max}$ decreases like $\frac{1}{t}$ where t is the time since the last instability at this location. This is, of course, just an ad hoc assumption.

A power-law distribution of the event sizes with a scaling exponent close to 2 was found, and it was theoretically shown that this exponent is independent of the driving rates r_u and r_v. The value $\alpha \approx 2$ was within the range of estimates of α_A for regolith landslides at that time and even in fair agreement with the apparently most reliable value $\alpha_A \approx 2.4$ suggested by Malamud et al. [2004].

The model suggested by Piegari et al. [2006a,b] is similar in its spirit, but differs in some details and, more importantly, concerning its dissipative character. The local variable is the inverse of the factor of safety (Eq. 4) and thus simply proportional to the local shear stress. Reasoned by the existence of several dissipative components in landsliding processes, such as evaporation of water or volume contractions, the authors skipped the conservation of stress and allowed an arbitrary degree of dissipation in the relaxation rule.

At this level, the model is just another physical interpretation of the OFC earthquake model. In extension of the OFC model, the authors replaced the infinitely slow long-term driving with a finite driving rate, as it was investigated by Hamon et al. [2002] in the context of solar flares. Furthermore, they introduced an anisotropic relaxation rule since stress transfer in direction of the slope may be stronger than perpendicular to the slope.

Power-law distributions for the event sizes were found for several combinations of the model parameters (dissipation, anisotropy, and driving rate), resulting in a rather large range of scaling exponents. The range includes the values found for regolith landslides in nature. In some cases, the power-law distribution was even lost. In a more recent paper [Piegari et al., 2009], the results of this model were quantitatively compared to some of the landslide inventories discussed in the previous section. The authors found combinations of the model parameters that reproduce both the scaling exponent and the rollover at small landslide sizes quite well after spatial scaling of the discrete, nondimensional model. However, the choice of the parameters and the spatial scale is based on a fit to the data, and there seems to be no way to derive this choice from physical principles so far. So it is still unclear why the model parameters should always be in a rather narrow range to yield similar landslide size distributions under strongly different conditions.

Despite the promising results obtained from the two models discussed in this section, some critical comments should be made. The first one mainly concerns the range of scaling exponents obtained from the model of Piegari et al. that is obviously much wider than the variation found in nature. This problem also concerns the original OFC model with respect to real earthquakes. In principle, the degree of dissipation introduces a tuning parameter which cannot be constrained using physical arguments.

The second criticism arises from the existing knowledge on the behavior of the OFC model. The occurrence of nearly periodic large events was soon discovered [Olami and Christensen, 1992], and recently a more or less complete understanding how the power-law distribution arises from the synchronization and the desynchronization of patches toppling almost periodically has been achieved [Hergarten and Krenn, 2011]. The organization towards an apparently critical state extends over many periods, so that these findings may even support the arguments against the applicability of the OFC model to real earthquakes. With respect to landslides, this argument may even be more severe as it is very difficult to imagine that the power-law distribution emerges after a long series of almost periodic sliding events involving parts of a slope. Due to its similarity with the OFC model, it can be expected that the nonconservative model of Piegari et al. behaves exactly like this. For the two-variable model of Hergarten and Neugebauer, there seems to be no further knowledge on its organization towards a critical state, but a similar behavior might be expected.

Finally, the question whether these mechanical models refer to the statistical distributions derived from landslide inventories at all should be taken into account. Since changes in topography are neglected in these models, they describe slip events with a small displacement on an individual slope. Such events have been subject of research in the last decades and may finally help to understand landslide dynamics or even help to predict large landslides, but the events recorded in landslide inventories take place on the landscape scale. Apparently very little is known about the size statistics of these small slip events, but even if they are power-law distributed it is not clear whether this distribution has any relation to the landslide distribution on the landscape scale.

3 Geomorphic Models

The second class of models attempting to relate landslides to SOC is part of the large group of landform evolution models. In these models, stresses in the material are not explicitly considered. Instead, slope instability is assumed to depend on properties of the relief, mainly on local slope. In a simplified view, these model approaches can be characterized by the key word sandpile dynamics. Apart form numerical modeling, this topic was also addressed in several laboratory experiments with different granular materials [e.g., Frette et al., 1996, Katz and Aharonov, 2006, Juanico et al., 2008].

In the context of sandpile dynamics, the Bak-Tang-Wiesenfeld (BTW) model [Bak et al., 1987, 1988] which was the first model of SOC and still seems to be some kind of paradigm should be mentioned first. This model is often denoted sandpile model, and even the entire class of models which are similar in their rules are often referred to as sandpile models.

For the two-dimensional BTW model, the presumably most reliable estimate on the scaling exponent of the avalanche size distribution in the limit of infinite system size is $\alpha = 1.27$ [Chessa et al., 1999]. Interestingly, this value is almost in the middle of the range $1.07 \leq \alpha_V \leq 1.52$ found for rockfalls and rockslides in nature. And as it should be no problem to accept sandpile dynamics as a simplified representation of rockslides, the problem of relating rockslides (and in principle rockfalls, too) to SOC seems to be solved.

However, the problem in this reasoning is not the question whether sandpile dynamics captures the processes relevant for rockslide dynamics, but the relationship between the BTW model and sandpile avalanches. In the BTW model, a site becomes unstable if its local variable becomes too large. This local variable is often considered as a number of grains at this site and may thus be seen as a representation of surface height. In contrast, the stability of a sandpile depends on the local slope gradient, which should be related to differences in the numbers of grains at neighbored sites instead of their absolute number. Furthermore, redistribution of grains in case of instability should not be isotropic as it is in the BTW model, but mainly in downslope direction.

To get around this fundamental problem, one may be tempted to skip the idea that the variable in the BTW model represents a number of grains, but interpret it as an abstract property that is somehow related to the slope of a sandpile. However, the attempt to relate this variable to slopes succeeds in one dimension, but quantitatively fails on a two-dimensional lattice [Hergarten, 2002, 2003]. So the BTW model provides a fundamental description of avalanche propagation on a rather abstract level, but a physically consistent relation to sandpile dynamics or any type of gravity-driven mass movements is not visible.

The presumably first geomorphic models to reproduce power-law statistics in landslide dynamics were published almost 15 years ago [Densmore et al., 1998, Hergarten and Neugebauer, 1998]. Compared to the most widespread models in the field of SOC, these models are rather complicated and involve several parameters.

The model of Hergarten and Neugebauer [1998] is based on partial differential equations. It contains two variables, the surface elevation $H(x_1,x_2,t)$ and the thickness of an upper mobile layer $\kappa(x_1,x_2,t)$, both being functions of the horizontal coordinates x_1 and x_2 and the time t. The material in the mobile layer flows at a velocity proportional to the slope of the surface if a given threshold is exceeded. This behavior is represented by the differential equation

$$\frac{\partial H}{\partial t} = \operatorname{div} \begin{cases} \alpha\,(\kappa|\nabla H| - \beta)\,\frac{\nabla H}{|\nabla H|} & \text{if} \quad \kappa|\nabla H| > \beta \\ 0 & \text{else} \end{cases} . \tag{9}$$

The parameter α is related to the flow velocity at given slope, while β defines the threshold where flow starts. The symbols div and ∇ refer to the two-dimensional divergence and gradient operators, respectively. It was further assumed that material from the lower solid layer becomes mobile at a (spatially and temporally) random rate r which is the only random component in the model. In return the thickness of the mobile layer decays with a given time constant τ. Furthermore, the entrainment of further material due to flow was taken into account. These phenomena were incorporated by the second differential equation

$$\frac{\partial}{\partial t}(H-\kappa) = -r + \frac{\kappa}{\tau} \underbrace{-\,\gamma\alpha\,(\kappa|\nabla H| - \beta)\,|\nabla H|}_{\text{if } \kappa|\nabla H|>\beta} \tag{10}$$

where the additional parameter γ quantifies the entrainment of material by flow. The model was applied to individual slopes, and long-term driving was introduced by a constant lowering at the toe of the slope mimicking the incision of a river.

At that time, the system of differential equations could only be solved with reasonable effort on lattices of no more than 64×64 sites. A power-law distribution of the landslide sizes was found over only one and a half order of magnitude in area. The authors analyzed cumulative distributions. Transferred to non-cumulative frequency densities, they obtained a scaling exponent $\alpha_A \approx 2.1$ which is not far off from the values found for regolith landslides. However, serious parameter studies have not been performed. So the question remains whether this model predicts a universal scaling exponent or whether there is a significant dependence on the model parameters. Apart from this, the geometry of the events seems not to be very realistic. As illustrated in Fig. 7, the landslides are rather long and tall and look even a little like gorges in direction of the slope.

The model of Densmore et al. [1998] is a rather comprehensive landform evolution model where landsliding is only one component beside fluvial sediment transport and diffusive slope processes. As a major difference towards the models discussed before, slope instability is not treated as a progressive phenomenon. Only the initiation of a landslide at any location is considered, while the size of the resulting event is completely determined by the existing topography and by an ad hoc rule. This topography is, in return, the result of all the processes considered in the model, including previous landslides.

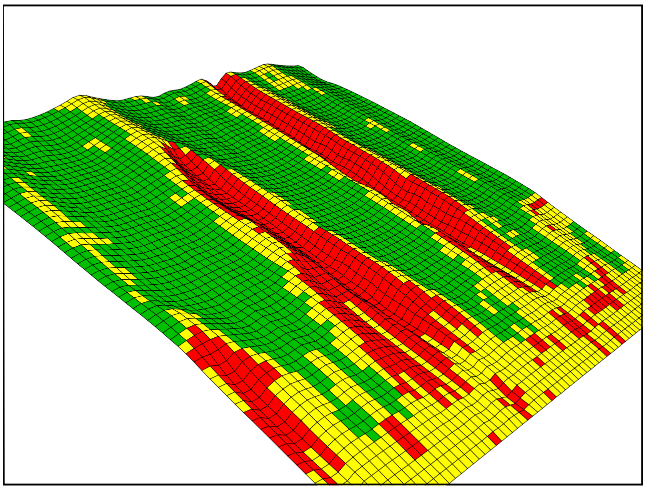

Fig. 7 Surface after a large landslide in the model of Hergarten and Neugebauer [1998]. Regions that were unstable are yellow; regions where a significant loss of height occurred (larger than the incision of the river) are red.

Compared to the model discussed above, the authors attempted to include more knowledge on the stability of real slopes instead of using ad hoc rules for the initiation of landslides. Most of this knowledge hinges on the concept of the factor of safety discussed in the previous section (Eq. 4) in combination with the Mohr-Coulomb failure criterion. This criterion is widely used in mechanics and states that failure occurs if the shear stress exceeds the maximum shear stress given by

$$\tau_{\max} = \sigma \tan\phi + C \tag{11}$$

where σ is the normal stress. The parameters ϕ and C describe the properties of the material where ϕ is the angle of internal friction and C is the cohesion. For the simplest case of a layer of constant thickness d on a potential failure plane inclined by an angle θ, the Mohr-Coulomb criterion immediately leads to

$$FS = \frac{\tan\phi}{\tan\theta} + \frac{C}{\rho g d \sin\theta} \tag{12}$$

where ρ is the density and g is the gravitational acceleration. This simple relationship is often used as a first estimate. It states that planes with angles of inclination $\theta < \phi$ are always stable, while cohesion even enables steeper planes to remain stable as long as the layer is thin.

Densmore et al. used this criterion to discriminate sites where landslides may be initiated and the maximum landslide volume at these locations. As they wanted landslides to be initiated only close to the toe of hillslopes, they searched the lowest pair of neighbored sites at each hillslope where the slope angle β between both is larger than ϕ. In Fig. 8 these two sites are colored yellow. In the next step, the authors used the Mohr-Coulomb criterion to estimate the maximum height difference H_c between these sites where the slope remains stable and related it to the actual height difference H. They assumed that failure occurs at a probability

$$p = \frac{H}{H_c} + rt \tag{13}$$

where t is the time since the last event at this site, and r gives the rate of increase in probability due to time-dependent weakening. In case of instability, a potential landslide volume is computed. For this, they made an estimate of the most likely plane of failure using the Mohr-Coulomb criterion and found that it dips at the angle $\theta = \frac{\beta+\phi}{2}$. The volume above this plane, colored red in Fig. 8, defines the maximum possible volume of a landslide at this hillslope. Based on their own empirical results [Densmore et al., 1997], they finally assumed that the real landslide volume is directly proportional to the time since the last landslide initiated at this location, limited by the maximum volume.

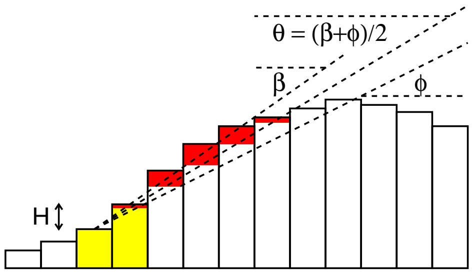

Fig. 8 Illustration of the landsliding algorithm suggested by Densmore et al. [1998]. Landslides can be initiated at the lowest pair of sites on a hillslope where the slope angle β exceeds ϕ (yellow). The maximum landslide volume (red) is defined by a plane that dips at an angle $\theta = \frac{\beta+\phi}{2}$.

Comparing the physical basis of the model with the number of ad hoc rules raises the question whether the physically-based part of the model has any effect on the results. But apart from this, the derivation of the most likely dip angle θ and the maximum stable height difference H_c are wrong. The authors considered the height difference H and the slope angle β between the considered sites as independent and claimed a quite large degree of freedom when deciding which one is variable and which one is given by the actual topography. So it is not surprising that their result on the maximum stable slope is not in agreement with the simple estimate given by Eq. 12.

Taking these aspects into account, the part of the model referring to landslides is just a combination of ad hoc rules, similarly to the model of Hergarten and Neugebauer discussed above, but more complicated. However, it should be kept in mind that such rules are not necessarily bad as long as they are reasonable and the results make sense. Similarly to Hergarten and Neugebauer, Densmore et al. obtained power-law distributions of the landslide sizes within a narrow range of scales. In two simulations involving different strength of the material (represented by ϕ and C) they found values $\alpha_V = 2.2$ and $\alpha_V = 1.8$ with respect to the volume over about one order of magnitude. These values are in very good agreement with the estimate

$\alpha_V \approx 2.0$ (or slightly larger, depending on the scaling between volume and area) for the volumes of real regolith landslides given in Eq. 3. The smaller scaling exponent occurred at higher strength, and this result goes even in the direction that the scaling exponent for rockfalls and rockslides is smaller than that of regolith landslides. However, this may also be a matter of fitting straight lines over rather narrow ranges, and if any error bars had been given, they would surely be larger than the difference between the two values.

After several years of apparent silence in this field, a new approach focusing on rockfalls (again including rockslides) has been recently published by Hergarten [2012]. This model is inspired by ideas on sandpile dynamics and extremely simple compared to the other models reviewed in this chapter. In return it is, however, more or less completely based on ad hoc rules. The basic assumption is that landslides can in principle be triggered at any site with a probability that depends on the local slope gradient. All other contributions to rock instability in nature such as fracturing are mimicked by the randomness of the triggering process.

In analogy to the fluvial erosion models mentioned in the introduction, the gradient at each site is computed in the direction of steepest descent among the eight (direct and diagonal) neighbors on a rectangular lattice, what is called D8 algorithm [O'Callaghan and Mark, 1984]. It is further assumed that slopes below a lower threshold slope $s_{\min}$ remain stable under all conditions, while slopes above an upper threshold slope $s_{\max}$ are destabilized by any impact. For slopes s between $s_{\min}$ and $s_{\max}$ a linear increase of the probability of instability in case of an impact is assumed:

$$p = \frac{s - s_{\min}}{s_{\max} - s_{\min}}. \tag{14}$$

If a site becomes unstable, material is removed until its slope decreases to $s_{\min}$. The downslope motion of unstable rock masses and their deposition is not computed, only the volume of detached material is recorded and used for the event size statistics. The effect of the event on its vicinity, i.e., progressive destabilization in the source area of the rockfall, is mimicked by exposing the eight neighbored sites to the same random impact as the unstable site, so that each of them may become unstable with a probability given by Eq. 14, too. Those sites which received an impact without becoming unstable are assumed to be stable at their present slope and cannot be destabilized by further impacts unless their slope increases as a consequence of further removal of material at neighbored sites. This is realized by replacing $s_{\min}$ of these sites by the present value of s.

In contrast to all the models discussed earlier, this model only simulates the occurrence and the size of rockfalls on a given relief. Long-term driving forces, mainly fluvial erosion in combination with tectonic uplift and, particularly important in the context of rockfalls, glacial erosion, are not considered. So if this model yields a power-law distribution of the rockfalls, it only shows that the relief it is applied to has critical properties with respect to this mechanism. In the context of SOC, this is clearly a disadvantage, but in return it might allow a hazard assessment for a given region which is not so easy with models bringing their own mechanism of long-term driving.

The model was applied to Digital Elevation Models of three mountain belts: the European Alps, the central part of the Himalayas, and the southern part of the Rocky Mountains. The elevation data were taken from the ASTER Global Digital Elevation Model (a product of METI and NASA) with a resolution of 1 arc second, corresponding to about 20–30 m.

As illustrated in Fig. 9, the model predicts a power-law distribution with a scaling exponent $\alpha_V = 1.35$ for all three regions, although they strongly differ in their topographic characteristics. This value falls perfectly into the range $1.07 \leq \alpha_V \leq 1.52$ found for rockfalls and rockslides. Significant differences between the regions only concern the cutoff behavior at large event sizes. The results shown in Fig. 9 were obtained using the parameter values $s_{\min} = 1$ and $s_{\max} = 5$, only justified by the rule of thumb that the majority of real rockfalls and rockslides occurs at slope angles greater than 45°. However, it was shown that a variation of the model parameters $s_{\min}$ and $s_{\max}$ within a reasonable range has a minor effect on the scaling exponent of the event-size distribution. Similarly to the differences between the considered regions, variations in the parameters mainly affect the cutoff behavior at large event sizes. The regional differences in the cutoff behavior were interpreted in terms of subcriticality of the present relief with respect to the model's mechanism. It was concluded that the Himalayas are closer to a critical state than the Alps, which are themselves closer to a critical state than the southern part of the Rocky Mountains.

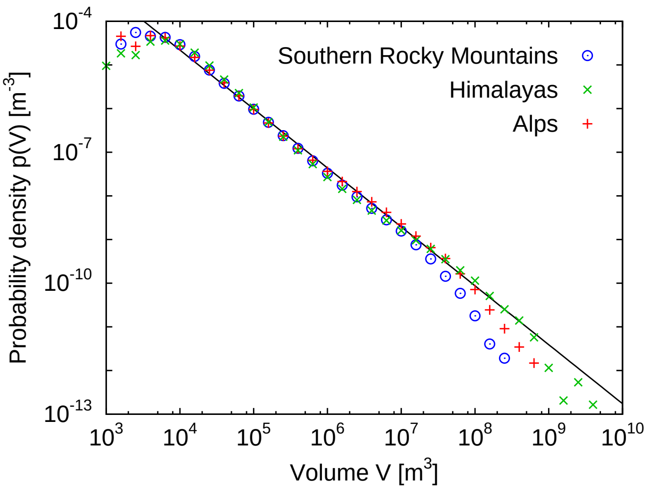

Fig. 9 Probability density of the rockfalls predicted by the model of Hergarten [2012] for the European Alps (43–48° N and 5–16° E), the central part of the Himalayas (26–31° N, 82–92° E) and for the southern part of the Rocky Mountains (35–45° N and from 105° W to the West Coast), computed with $s_{\min} = 1$ and $s_{\max} = 5$. The straight line corresponds to a power-law distribution with an exponent $\alpha_V = 1.35$.

In the same paper, a first attempt do derive a topography-based rockfall hazard map from the model was also made. The map presented in Fig. 10 is based on a prediction of a 2000 year time span and shows a rather inhomogeneous distribution of the hazard in the European Alps. The largest predicted event is illustrated in Fig. 11. It involves a volume of about 0.5 km^3 and is predicted to occur with a rather high probability of one per 500 years. However, it was already admitted in the original paper that quantitative assessments based on this model must be treated with some caution. First, assigning an absolute time scale to the model is rather uncertain. And second, variations in the parameters s_{min} and s_{max} which can only be guessed so far have a stronger influence on the largest events than on the power-law distribution itself. It was already discussed in the original paper that even a small increase in s_{min} and s_{max} by 20 % reduces both the size and the probability of occurrence of the largest events by a factor of two. Even stronger regional variations in these parameters can be expected due to lithology, so that in particular estimating the size and frequency of the largest events in a mountain belt seems to be rather uncertain. So this model may provide a tool for hazard assessment, but any serious application requires additional data that cannot be derived vom physical principles in a straightforward way.

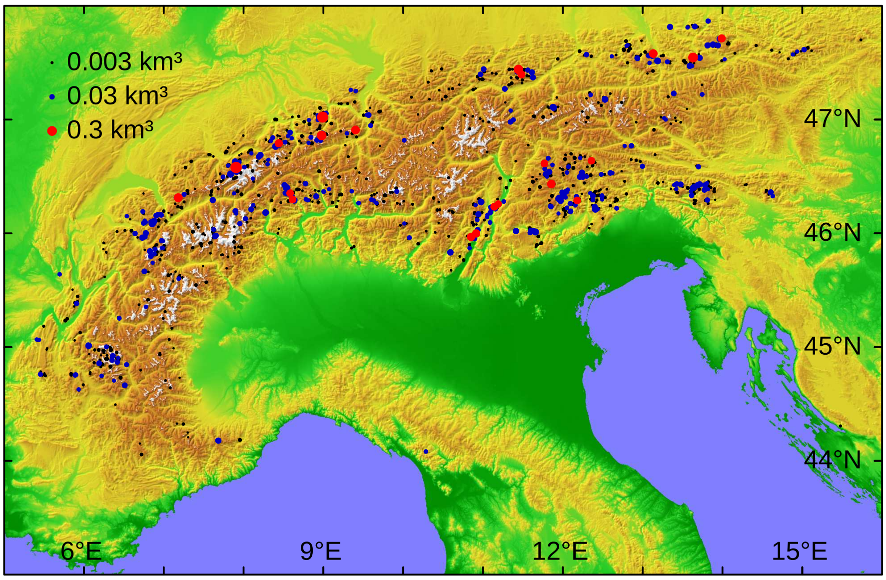

Fig. 10 Rockfalls with $V \geq 10^{-3}$ km^3 predicted for a 2000 year time span in the Alps [Hergarten, 2012]. Black: $V \in [0.001, 0.01)$ km^3 (756 events), blue: $V \in [0.01, 0.1)$ km^3 (301 events), red: $V \geq 0.1$ km^3 (21 events).

Nevertheless, the model seems to have a large potential for both application to rockfall hazard assessment and for clarifying the role of SOC in rockfall dynamics. But as mentioned above, the latter first requires an extension of the model by long-term driving processes such as fluvial or glacial erosion that locally steepen the relief and thus supply the potential for mass movements.

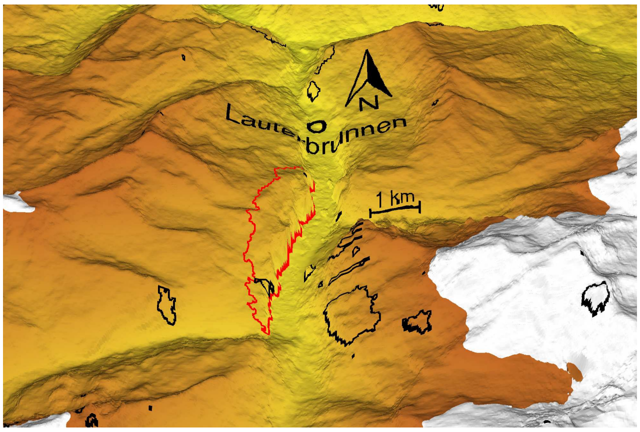

Fig. 11 The largest event predicted for the Alps (Lauterbrunnen valley, $V \approx 0.5$ km^3, red). The black lines correspond to smaller events predicted for a 2000 year time span.

To summarize, there is growing evidence for power-law size distributions in different types of landslides. The scaling exponents found for regolith landslides strongly differ from those found for rockfalls and rockslides, but each of this classes may be characterized by a universal scaling exponent. A handful of models has been designed to reproduce these power-law distributions. Most of them address regolith landslides, an all hinge on ad hoc rules. So far none of them provides a consistent explanation for the difference in the scaling exponents found for different types of landslides. Even none of them can uniquely identify any type of landsliding as a phenomenon governed by SOC, but this applies to almost all natural phenomena considered in the context of SOC.

References

P. Bak. *How Nature Works – the Science of Self-Organized Criticality*. Copernicus, Springer, Berlin, Heidelberg, New York, 1996.

P. Bak, C. Tang, and K. Wiesenfeld. Self-organized criticality. An explanation of 1/f noise. *Phys. Rev. Lett.*, 59:381–384, 1987. doi: 10.1103/PhysRevLett.59.381.

P. Bak, C. Tang, and K. Wiesenfeld. Self-organized criticality. *Phys. Rev. A*, 38: 364–374, 1988. doi: 10.1103/PhysRevA.38.364.

M. T. Brunetti, F. Guzetti, and M. Rossi. Probability distribution of landslide volumes. *Nonlin. Processes Geophys.*, 16:179–188, 2009.

R. Burridge and L. Knopoff. Model and theoretical seismicity. *Bull. Seismol. Soc. Am.*, 57:341–371, 1967.

A. Chessa, H. E. Stanley, A. Vespignani, and S. Zapperi. Universality in sandpiles. *Phys. Rev. E*, 59:R12–R16, 1999.

A. L. Densmore, R. S. Anderson, B.G. McAdoo, and M. A. Ellis. Hillslope evolution by bedrock landslides. *Science*, 275:369–372, 1997.

A. L. Densmore, M. A. Ellis, and R. S. Anderson. Landsliding and the evolution of normal-fault-bounded mountains. *J. Geophys. Res.*, 103:15203–15219, 1998.

L. K. A. Dorren. A review of rockfall mechanics and modelling approaches. *Progress in Physical Geography*, 1:69–87, 2003.

C. Dussauge, A. Helmstetter, J.-R. Grasso, D. Hantz, P. Desvarreux, M. Jeannin, and A. Giraud. Probabilistic approach to rock fall hazard assessment: potential of historical data analysis. *Natural Hazards and Earth System Sciences*, 2:15–26, 2002.

I. S. Evans and C. J. McClean. The land surface is not unifractal: variograms, cirque scale and allometry. *Z. Geomorph. N. F.*, Suppl. 101:127–147, 1995.

J. Feder. *Fractals*. Plenum Press, New York, 1988.

V. Frette, K. Christensen, A. Malthe-Sørenssen, J. Feder, T. Jøssang, and P. Meakin. Avalanche dynamics in a pile of rice. *Nature*, 379:49–52, 1996.

Y. Fuyii. Frequency distribution of the magnitude of landslides caused by heavy rainfall. *Seismol. Soc. Japan J.*, 22:244–247, 1969.

F. Guzzetti, P. Reichenbach, and G. F. Wieczorek. Rockfall hazard and risk assessment in the Yosemite Valley, California, USA. *Natural Hazards and Earth System Sciences*, 3:491–503, 2003.

F. Guzzetti, P. Reichenbach, and S. Ghigi. Rockfall hazard and risk assessment in the Nera River Valley, Umbria, Region, central Italy. *Environ. Manage.*, 34: 198–208, 2004.

J. T. Hack. *Studies of longitudinal profiles in Virginia and Maryland*. Number 294-B in US Geol. Survey Prof. Papers. US Government Printing Office, Washington D.C., 1957.

D. Hamon, M. Nicodemi, and H. J. Jensen. Continuously driven OFC: A simple model of solar flare statistics. *Astronomy & Astrophysics*, 387:326–334, 2002.

S. Hergarten. *Self-Organized Criticality in Earth Systems*. Springer, Berlin, Heidelberg, New York, 2002.

S. Hergarten. Landslides, sandpiles, and self-organized criticality. *Natural Hazards and Earth System Sciences*, 3:505–514, 2003.

S. Hergarten. Topography-based modeling of large rockfalls and application to hazard assessment. *Geophys. Res. Lett.*, 39:L13402, 2012. doi: 10.1029/2012GL052090.

S. Hergarten and R. Krenn. Synchronization and desynchronization in the Olami-Feder-Christensen earthquake model and potential implications for real seismicity. *Nonlin. Processes Geophys.*, 18:635–642, 2011. doi: 10.5194/npg-18-635-2011.

S. Hergarten and H. J. Neugebauer. Self-organized criticality in a landslide model. *Geophys. Res. Lett.*, 25:801–804, 1998.

S. Hergarten and H. J. Neugebauer. Self-organized criticality in two-variable models. *Phys. Rev. E*, 61:2382–2385, 2000.

S. Hergarten and H. J. Neugebauer. Self-organized critical drainage networks. *Phys. Rev. Lett.*, 86:2689–2692, 2001.

R. E. Horton. Erosional development of streams and their drainage basins; hydrophysical approach to quantitative morphology. *Bull. Geol. Soc. Am.*, 56:275–370, 1945.

N. Hovius, C. P. Stark, and P. A. Allen. Sediment flux from a mountain belt derived by landslide mapping. *Geology*, 25:231–234, 1997.

O. Hungr, S. G. Evans, and J. Hazzard. Magnitude and frequency of rock falls along the main transportation corridors of southwestern British Columbia. *Can. Geotechn. J.*, 36:224–238, 1999.

H. J. Jensen. *Self-Organized Criticality – Emergent Complex Behaviour in Physical and Biological Systems*. Cambridge University Press, Cambridge, New York, Melbourne, 1998.

D. E. Juanico, A. Longjas, R. Batac, and C. Monterola. Avalanche statistics of driven granular slides in a miniature mound. *Geophys. Res. Lett.*, 35:L19403, 2008. doi: 10.1029/2008GL035567.

O. Katz and E. Aharonov. Landslides in vibrating sand box: What controls types of slope failure and frequency magnitude relations? *Earth. Planet. Sci. Lett.*, 247: 280–294, 2006. doi: 10.1016/j.epsl.2006.05.009.

A. E. Klar, E. Aharonov, B. Kalderon-Asael, and O. Katz. Analytical and observational relations between landslide volume and surface area. *J. Geophys. Res.*, 116:F02001, 2011. doi: 10.1029/2009JF001604.

S. Kramer and M. Marder. Evolution of river networks. *Phys. Rev. Lett.*, 68:381–384, 1992.

A. Kühni and O. A. Pfiffner. The relief of the Swiss Alps and adjacent areas and its relation to lithology and structure: topographic analysis from a 250-m DEM. *Geomorphology*, 41:285–307, 2001.

B. D. Malamud, D. L. Turcotte, F. Guzzetti, and P. Reichenbach. Landslide inventories and their statistical properties. *Earth Surface Processes and Landforms*, 29: 687–711, 2004.

B. B. Mandelbrot. How long is the coast of Britain? Statistical self-similarity and fractional dimension. *Science*, 156:636–638, 1967.

B. B. Mandelbrot. *The Fractal Geometry of Nature*. W. H. Freeman & Co., San Francisco, 1982.

B. B. Mandelbrot. Self-affine fractals and fractal dimension. *Physica Scripta*, 32: 257–260, 1985.

D. A. Noever. Himalayan sandpiles. *Phys. Rev. E*, 47:724–725, 1993.

J. F. O'Callaghan and D. M. Mark. The extraction of drainage networks from digital elevation data. *Computer Vision, Graphics, and Image Processing*, 28:323–344, 1984.

Z. Olami and K. Christensen. Temporal correlations, universality, and multifractality in a spring-block model of earthquakes. *Phys. Rev. A*, 46:R1720–R1723, 1992.

Z. Olami, H. J. S. Feder, and K. Christensen. Self-organized criticality in a continuous, nonconservative cellular automation modeling earthquakes. *Phys. Rev. Lett.*, 68:1244–1247, 1992. doi: 10.1103/PhysRevLett.68.1244.

E. Piegari, V. Cataudella, R. Di Maio, L. Milano, and M. Nicodemi. A cellular automaton for the factor of safety field in landslides. *Geophys. Res. Lett.*, 33: L01403, 2006a.

E. Piegari, V. Cataudella, R. Di Maio, L. Milano, and M. Nicodemi. Finite driving rate and anisotropy effects in landslide modeling. *Phys. Rev. E*, 73:026123, 2006b.

E. Piegari, R. Di Maio, and L. Milano. Characteristic scales in landslide modelling. *Nonlinear Processes in Geophysics*, 16:515–523, 2009. doi: 10.5194/npg-16-515-2009.

A. Rinaldo, I. Rodriguez-Iturbe, R. Rigon, and R. L. Bras. Self-organized fractal river networks. *Phys. Rev. Lett.*, 70:822–825, 1993.

V. B. Sapozhnikov and E. Foufoula-Georgiou. Do the current landscape evolution models show self-organized criticality? *Water Resour. Res.*, 32:1109–1112, 1996.

V. B. Sapozhnikov and E. Foufoula-Georgiou. Experimental evidence of dynamic scaling and indications of self-organized criticality in braided rivers. *Water Resour. Res.*, 33:1983–1991, 1997.

D. S. Simonett. Landslide distribution and earthquakes in the Beweni and Torricelli Mountains, New Guinea. In J. N. Jennings and J. A. Mabutt, editors, *Landform Studies from Australia and New Guinea*, pages 64–84. Cambridge University Press, Cambridge, 1967.

A. N. Strahler. Hypsometric (area-altitude) analysis of erosional topography. *Bull. Geol. Soc. Am.*, 63:1117–1142, 1952.

H. Takayasu and H. Inaoka. New type of self-organized criticality in a model of erosion. *Phys. Rev. Lett.*, 68:966–969, 1992.

A. Volkwein, K. Schellenberg, V. Labiouse, F. Agliardi, F. Berger, F. Bourrier, L. K. A. Dorren, W. Gerber, and M. Jaboyedoff. Rockfall characterisation and structural protection – a review. *Nat. Hazards Earth Syst. Sci.*, 11:2617–2651, 2011. doi: doi:10.5194/nhess-11-2617-2011.

A. von Poschinger. The Flims rockslide dam. In S. G. Evans, R. L. Hermanns, A. Strom, and G. Scarascia-Mugnozza, editors, *Natural and artificial rockslide dams*, pages 407–421. Springer, Berlin, Heidelberg, New York, 2011.

R. F. Voss. Random fractal forgeries. In R. A. Earnshaw, editor, *Fundamental Algorithms in Computer Graphics*, pages 805–835. Springer, Berlin, Heidelberg, New York, 1985.